Article:
Penfold, N.J.W., Whatley, J.R. and Armes, S.P. (2019) Thermoreversible block copolymer worm gels using binary mixtures of PEG stabilizer blocks. Macromolecules, 52 (4). pp. 1653-1662. ISSN: 0024-9297

https://doi.org/10.1021/acs.macromol.8b02491

Thermoreversible Block Copolymer Worm Gels

Using Binary Mixtures of PEG Stabilizer Blocks

Nicholas J. W. Penfold, Jessica Whatley and Steven P. Armes**

Department of Chemistry, Dainton Building, University of Sheffield,

Brook Hill, Sheffield, South Yorkshire, S3 7HF, UK.

Abstract. Two trithiocarbonate-based poly(ethylene glycol) (PEG) macromolecular chain transfer agents (macro-CTAs) with mean degrees of polymerization of 45 and 113 were prepared with ≥ 94% chain-end functionality. Binary mixtures of these PEG-trithiocarbonate macro-CTAs were then chain-extended *via* reversible addition-fragmentation chain transfer (RAFT) aqueous dispersion polymerization of 2-hydroxypropyl methacrylate (HPMA). Systematic variation of the relative proportions of PEG_{45} and PEG_{113} macro-CTAs and the degree of polymerization of the PHPMA core-forming block resulted in the formation of [x PEG_{45} + z PEG_{113}] - $PHPMA_n$ block copolymer spheres, worms or vesicles, where x and z represent the mol fractions of PEG_{45} and PEG_{113}, respectively. A phase diagram was constructed to establish the relationship between block copolymer composition and nanoparticle morphology. The thermoresponsive behavior of block copolymer worms was assessed by visual inspection, DLS, transmission electron microscopy (TEM) and temperature-dependent oscillatory rheology. Increasing the proportion of PEG_{45} (x = 0.00 to 0.40) in the stabilizer block resulted in a moderate increase in worm gel strength, but cooling resulted in *irreversible* degelation owing to a worm-to-sphere morphology transition. However, the phase diagram enabled identification of a diblock copolymer composition that exhibited *reversible* degelation behavior in pure water. This formulation was then further optimized to exhibit the same rheological behavior in a commercial cell culture medium (*Nutristem*) by fixing the PEG mol fraction at x = 0.70 while lowering the PHPMA DP from 115 to 75. Importantly, the gel strength at physiological temperature can be readily tuned simply by variation of the copolymer concentration. In principle, this study has important implications for the preservation of human stem cells, which can enter stasis when immersed in certain worm gels (see I. Canton *et al.*, *ACS Central Science*, **2016**, *2*, 65-74).

Introduction

Polymerization-induced self-assembly (PISA) has become widely recognized as a powerful platform technology for the rational synthesis of bespoke block copolymer nano-objects.[1-12] Much of the PISA literature involves reversible addition-fragmentation chain transfer (RAFT) polymerization,[13-18] but atom transfer radical polymerization (ATRP),[19-22] ring-opening metathesis polymerization (ROMP)[23-25] and nitroxide-mediated polymerization (NMP) can also be utilized.[26-30] PISA syntheses can be conducted at copolymer concentrations of up to 50% w/w in aqueous media,[31] and final monomer conversions of more than 99% are typically achieved.[32] For such formulations, a water-soluble polymer is chain-extended using either a water-immiscible monomer (aqueous emulsion polymerization)[33-35] or a water-miscible monomer (aqueous dispersion polymerization).[4] In each case the growing second block becomes water-insoluble at some critical degree of polymerization (DP), which drives the *in situ* block copolymer self-assembly. In principle, aqueous emulsion polymerization is applicable to a much wider range of vinyl monomers, but in practice such syntheses are often restricted to kinetically-trapped spheres.[36] In contrast, aqueous dispersion polymerization usually produces the full range of block copolymer nano-objects (i.e., spheres, worms or vesicles) if an appropriate PISA formulation is selected.[4, 37] Moreover, such nano-objects are much more likely to be stimulus-responsive, because the structure-directing water-insoluble block is only weakly hydrophobic.[11] For example, poly(glycerol monomethacrylate)-poly(2-hydroxypropyl methacrylate) (PGMA-PHPMA) worms form free-standing hydrogels at 20 °C owing to multiple contacts between neighboring worms.[38] Such gels undergo degelation on cooling as a result of a worm-to-sphere transition induced by surface plasticization. This thermal transition is fully reversible, which enables convenient sterilization *via* cold ultrafiltration.[39] Moreover, such hydrogels can be used

as biocompatible scaffolds for the 3D culture of various cell lines.[40] Interestingly, human stem cell colonies immersed in such hydrogels undergo stasis: they become non-proliferative and can survive in their naïve undifferentiated state for up to two weeks without passaging at 37 °C.[41] This suggests that such hydrogels may prove to be a useful storage medium for the global transport of human stem cells without cryopreservation.

Recently, we and others have explored the PISA synthesis of analogous diblock copolymer nano-objects in which the hydrophilic PGMA stabilizer block is replaced by poly(ethylene glycol) (PEG).[42-51] However, if the PEG block is relatively long (e.g. DP = 113), then PEG-PHPMA worms exhibit thermoresponsive but not thermoreversible behavior. In other words, degelation occurs on cooling to 5 °C, but regelation does not occur on returning to ambient temperature. Presumably, this is because the steric stabilization conferred by the PEG_{113} chains is sufficiently strong that multiple 1D sphere-sphere fusion does not occur on normal experimental time scales. This limitation prevents the evaluation of PEG-PHPMA worm gels in the context of human stem cell preservation. This is unfortunate, because comparing PEG-PHPMA and PGMA-PHPMA worm gels should shed light on the stasis mechanism. More specifically, do human stem cells enter their dormant state simply because these worm gels are very soft (the bulk modulus, G' is typically 10-50 Pa) or are chemical cues also important?

It is well-known in the PISA literature that the judicious use of binary mixtures of steric stabilizer blocks in PISA formulations can provide some useful advantages.[52-57] For example, using a binary mixture of short and long poly(methacrylic acid) stabilizers enables the rational synthesis of relatively small vesicles with narrow size distributions via RAFT dispersion polymerization of benzyl methacrylate in ethanol.[58] Similarly, combining a polyelectrolytic steric stabilizer with a non-ionic steric stabilizer is arguably the most convenient approach for the

preparation of either cationic or anionic block copolymer nanoparticles directly in aqueous media.

In the present study, we use a binary mixture of a relatively long PEG_{113} chain transfer agent (CTA) and a relatively short PEG_{45} CTA for the RAFT aqueous dispersion polymerization of HPMA. Our primary objective was to identify one or more PISA formulations that would enable PEG-PHPMA worms to exhibit *thermoreversible* (de)gelation behavior. If successful, such worm gels could be utilized to probe the mechanism by which naïve human stem cells enter stasis.

Results and Discussion

The use of linear PEG as a steric stabilizer block in PISA has received considerable interest over the past few years.[42-51, 59-64] The majority of the literature focuses on PEG macro-CTAs with a mean DP of either 45 or 113, primarily owing to the commercial availability of the corresponding monomethoxy PEG precursors. For example, Warren *et al.*[46] prepared PEG_{113}-$PHPMA_n$ diblock copolymer spheres, worms or vesicles at 50 °C, with oligolamellar vesicles being obtained at high copolymer concentrations for this formulation. Subsequently, PEG_{113}-$PHPMA_n$ vesicles have been evaluated as nanoreactors[48] or used to encapsulate therapeutic enzymes to enhance their proteolytic stability and minimize antibody recognition.[49] Blackman *et al.* used the same PISA formulation as a model to examine the fidelity of trithiocarbonate (TTC) end-groups, where PEG_{113}-$PHPMA_n$ nano-objects were prepared by either photoinitiation or thermal initiation.[47] Photoinitiation resulted in loss of the TTC end-groups, but also led to the formation of higher order morphologies. In related work, Tan *et al.*[50] demonstrated that PEG_{113}-$PHPMA_n$ spheres, worms or vesicles could be conveniently prepared using photo-PISA at 25 °C. Such mild conditions facilitated the *in situ* encapsulation of bovine serum albumin within

vesicles with retention of this cargo's catalytic activity. Furthermore, silica-loaded pH-responsive vesicles were synthesized by the same research group by statistically copolymerizing 2-(dimethylamino)ethyl methacrylate within the membrane-forming block.[43]

Ren and Perez-Mercader[44] also exploited photo-PISA to prepare PEG_{45}-$PHPMA_n$ diblock copolymer nano-objects in water at 25 °C. In this case, the PEG_{45} macro-CTA contained a hydrophobic *n*-dodecyl group, which resulted in the formation of PEG_{45}-$C_{12}H_{25}$ micelles in the aqueous reaction solution prior to the HPMA polymerization. Interestingly, sterically-stabilized nanoparticles were obtained but only for target PHPMA DPs of between 60 and 80. PEG_{45}-$PHPMA_{80}$ spheres formed free-flowing fluids at 15 °C and strong, free-standing gels at 40 °C. This sol-gel transition was apparently induced by the formation of a "micelle-network" rather than a sphere-to-worm morphology transition. However, such gel strengths appear to be too high for such hydrogels to be used for the long-term storage of stem cells.[41]

Synthesis of PEG macro-CTAs

Two poly(ethylene glycol) trithiocarbonate (PEG) macro-CTAs with mean DPs of 45 and 113 were synthesized *via* Steglich esterification from their monomethoxy precursors using a carboxylic acid-functionalized RAFT agent PETTC (Scheme 1). After purification, mean degrees of esterification of 94% and 95% were calculated for PEG_{45} and PEG_{113} respectively, by comparison of the integrated oxyethylene protons assigned to PEG at 3.3-4.4 ppm to that of the aromatic end-group at 7.2-7.4 ppm (see Figures S1A and S2A). THF GPC analysis indicated M_n = 2.5 kg mol^{-1} and M_w/M_n = 1.03 for the PEG_{45} macro-CTA and M_n = 5.8 kg mol^{-1} and M_w/M_n = 1.03 for the PEG_{113} macro-CTA (see Figures S1B and S2B). Binary mixtures of these macro-

CTAs were used to prepare [*x* PEG_{45} + *z* PEG_{113}] - $PHPMA_n$ diblock copolymer nanoparticles *via* RAFT aqueous dispersion polymerization of HPMA at 50 °C.

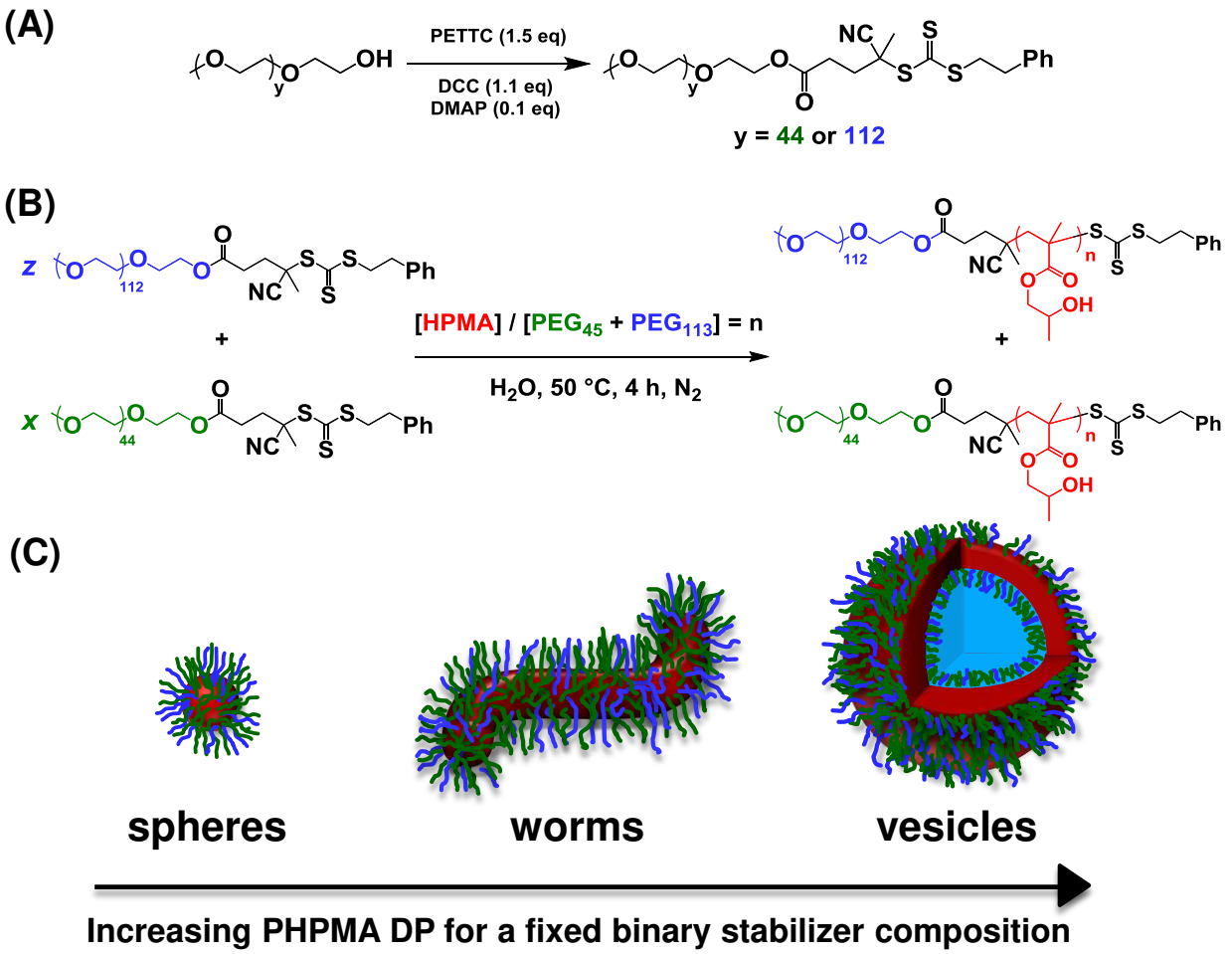

Scheme 1. (A) Reaction scheme for the synthesis of two PEG macro-CTAs with mean DPs of 45 and 113 *via* Steglich esterification. (B) Reaction scheme for the RAFT aqueous dispersion polymerization of HPMA at 50 °C for the synthesis of [*x* PEG_{45} + *z* PEG_{113}] - $PHPMA_n$ diblock copolymer nano-objects. (C) Schematic cartoon of the block copolymer spheres, worms and vesicles that can be accessed using this PISA formulation. The green and blue stabilizer chains represent PEG_{45} and PEG_{113}, respectively.

Synthesis of [*z* PEG_{113} + *x* PEG_{45}] - $PHPMA_n$ diblock copolymers

A series of [*x* PEG_{45} + *z* PEG_{113}] - $PHPMA_n$ diblock copolymer nanoparticles were synthesized by systematically varying the PEG mol fractions (*x* and *z*) and the target PHPMA DP (n). Table S1 summarizes the targeted diblock copolymer compositions, HPMA monomer conversions, molecular weight data and morphological assignments. More than 99% HPMA conversion was obtained in all cases, as calculated by ^{1}H NMR spectroscopy. An assigned ^{1}H NMR spectrum for [0.70 PEG_{45} + 0.30 PEG_{113}] - $PHPMA_{115}$ dissolved in CD_3OD after lyophilization is shown in Figure 1. The block copolymer composition was confirmed by comparing the integrated signals for the oxyethylene protons assigned to the PEG chains at 3.50-3.70 ppm to that for the methacrylic backbone of the PHPMA block at 0-2.50 ppm. The molecular weight distribution of each block copolymer was assessed by THF GPC using a series of near-monodisperse poly(methyl methacrylate) calibration standards. Unimodal chromatograms were obtained for most block copolymer compositions (see Figure S3 for examples). For $0 \leq x \leq 0.90$, lower M_n values are observed as more PEG_{45} is incorporated into the nanoparticle corona when targeting a fixed PHPMA DP. This is expected, as a higher mol fraction of PEG_{45} reduces the mean molecular weight for the binary stabilizer block. However, a unimodal chromatogram was not observed when PEG_{45} was used as the sole macro-CTA (i.e. for $x = 1.0$). Instead, a bimodal molecular weight distribution was obtained with a broad high molecular weight feature and a relatively narrow low molecular weight component (see Figure S3B). In a successful PISA synthesis, the water-soluble PEG macro-CTA confers effective steric stabilization (Scheme S1A).[4] However, sterically-stabilized nanoparticles were not obtained when using the PEG_{45} macro-CTA alone, even for the lowest targeted PHPMA DP of 100.

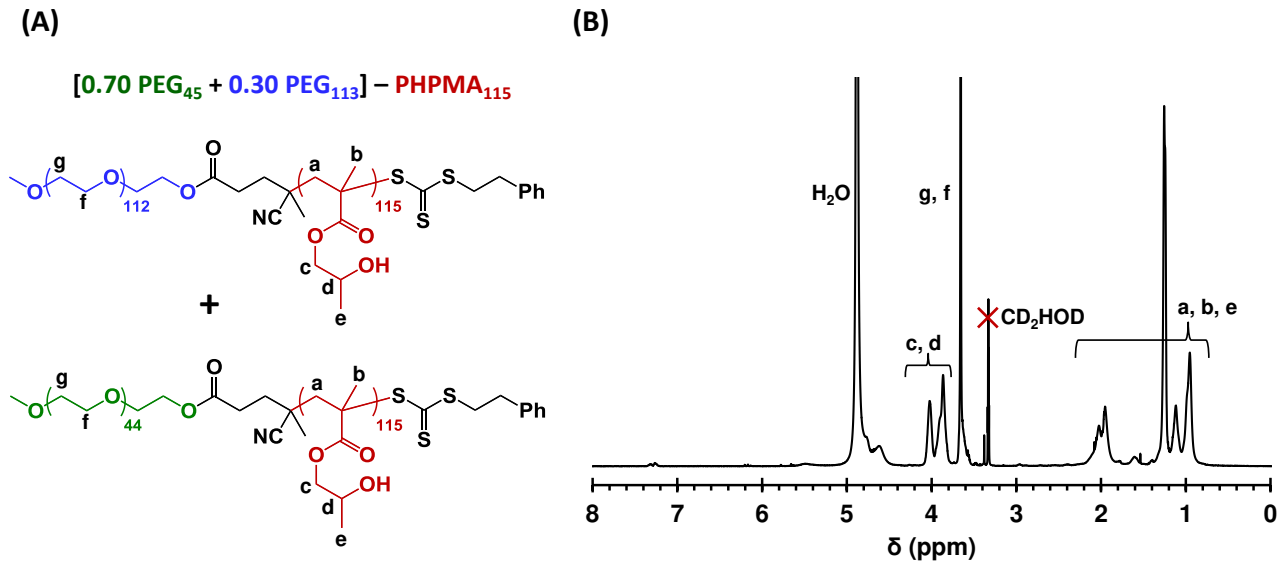

Figure 1. (A) Chemical structures and (B) assigned ^{1}H NMR spectrum (CD_3OD) for a [0.70 PEG_{45} + 0.30 PEG_{113}] - $PHPMA_{115}$ diblock copolymer.

In each case, phase separation occurred to produce a yellow solid phase and a turbid aqueous phase containing white precipitate. Subsequent ^{1}H NMR spectroscopy studies confirmed that the former component corresponded to PEG_{45}-$PHPMA_n$ diblock copolymer, whereas the latter component was simply PHPMA homopolymer. We propose the following mechanism (see Scheme S1B). Initially, the PEG_{45} macro-CTA is chain-extended with HPMA to yield water-soluble diblock copolymer chains. However, these growing PEG_{45}-$PHPMA_n$ chains then precipitate at the point of micellar nucleation, because the PEG_{45} block is not sufficiently long to act as an effective steric stabilizer at the reaction temperature of 50 °C. This accounts for the formation of the yellow precipitate. At this point, unreacted HPMA monomer remaining in the aqueous phase reacts with the water-soluble azo initiator, undergoing conventional free radical polymerization to produce highly polydisperse PHPMA homopolymer in the form of a white precipitate. In this context, it is noteworthy that photo-PISA formulations conducted at 25 °C

enable the synthesis of well-defined, colloidally stable PEG_{45}-$PHPMA_n$ diblock copolymer nano-objects.[44] This is because PEG exhibits inverse temperature solubility behavior:[65] it is a more effective steric stabilizer at lower temperature simply because it is more solvated under such conditions. However, we wished to target relatively soft PEG-based worm gels that (i) exhibit thermoreversible behavior and (ii) remain colloidally stable at 37 °C in the presence of various cell culture media. The latter requirement means that PEG_{45}-$PHPMA_n$ worms prepared via photo-PISA at 25 °C are unlikely to be suitable for the intended stem cell biology application. In principle, this technical problem can be addressed by using a judicious binary mixture of PEG_{113} and PEG_{45} macro-CTAs, as outlined in the present study.

Transmission electron microscopy (TEM) studies were performed on each diblock composition to assign the copolymer morphology. The resulting phase diagram constructed for [x PEG_{45} + z PEG_{113}] - $PHPMA_n$ is shown in Figure 2. When x = 0, PEG_{113}-$PHPMA_n$ diblock copolymer chains self-assemble to form spheres, worms or vesicles, depending on the precise PHPMA DP and vesicles occupy relatively broad phase space.[46] For all target PHPMA DPs, such self-assembly behavior remained more or less unchanged up to x = 0.30. However, when targeting a PHPMA DP of 150, the copolymer morphology switched from spheres to worms as x is increased from 0.30 to 0.40. This morphology transition is not unexpected, because increasing the mol fraction of the relatively short PEG_{45} macro-CTA reduces the effective volume fraction for the stabilizer chains in the corona.[66] Interestingly, a new 'rose-like' morphology was observed for PHPMA DPs of 150 – 250 but only for PEG_{45}-rich compositions (x = 0.80 or 0.90).

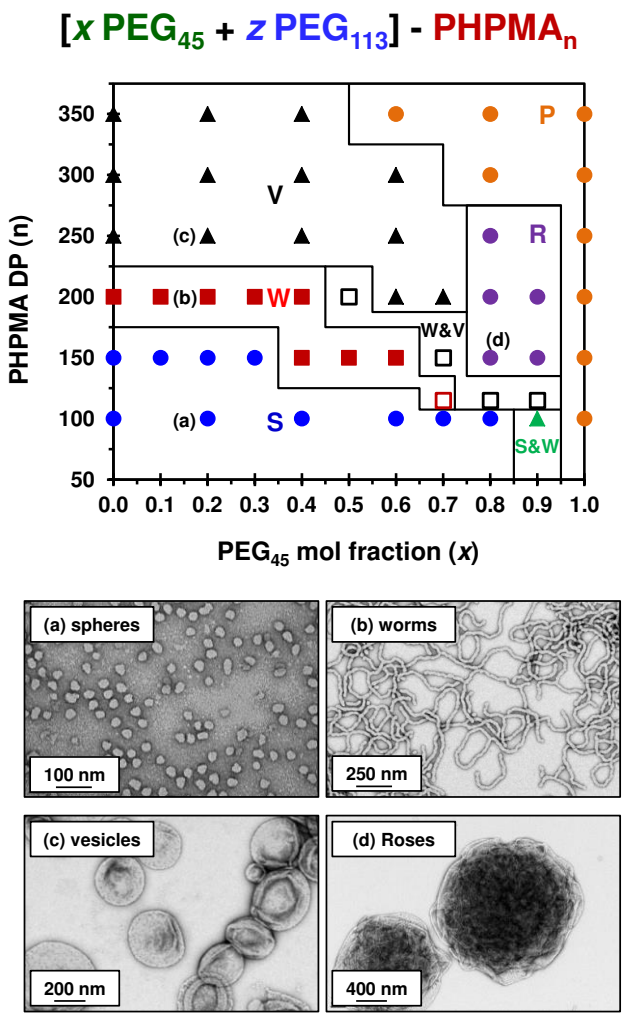

Figure 2. Phase diagram constructed for the RAFT aqueous dispersion polymerization of HPMA at 50 °C using a binary mixture of PEG_{113} and PEG_{45} macro-CTAs at 10% w/w solids [S = spheres, W = worms, R = roses V = vesicles, P = precipitate]. The general formula for this phase diagram is [*x* PEG_{45} + *z* PEG_{113}] – $PHPMA_n$, where n is the PHPMA DP and *x* and *z* are the mol fractions of PEG_{113} and PEG_{113} stabilizer chains, respectively. The filled red squares indicate diblock copolymer worms that undergo *irreversible* degelation on cooling to 4 °C. This thermal transition proved to be *reversible* for the single diblock composition indicated by the open red square. Four representative TEM images are shown for (a) spheres where *x* = 0.20 and *n* = 150,

(b) worms where $x = 0.20$ and $n = 200$ and (c) vesicles where $x = 0.20$ and $n = 250$ and (d) roses where $x = 0.80$ and $n = 150$.

Furthermore, targeting longer PHPMA DPs (i.e. 300 or 350) for these higher x values always resulted in precipitation, as the PEG_{45}-rich stabilizer composition is incapable of conferring sufficient steric stabilization. Macroscopic phase separation was also observed in all cases when $x = 1.0$, for the same reason (as discussed above). Importantly, a pure worm phase was obtained when targeting a PHPMA DP of 200 for $0.00 \leq x \leq 0.40$. For $x = 0.50$ or 0.60, worms could also be obtained by reducing the PHPMA DP to 150. However, for $x = 0.70$, worms could only be obtained at a PHPMA DP of 115. Thus, as the proportion of the relatively short PEG_{45} macro-CTA is increased, the volume fraction of stabilizer chains in the coronal layer is gradually reduced, which means that the volume fraction of the hydrophobic PHPMA block required to access the worm phase is correspondingly lower.

Analysis of the thermoresponsive behavior of PEG-based diblock copolymer worm gels

As-synthesized 10% w/w aqueous dispersions of [x PEG_{45} + z PEG_{113}] – $PHPMA_n$ worms were subjected to a thermal cycle to assess their thermoresponsive behavior. Firstly, each dispersion was cooled to 4 °C overnight followed by incubation at 25 °C for 24 h. Visual inspection (plus DLS and TEM studies of the PEG_{113}-$PHPMA_{200}$ dispersion)[46] indicated that this thermal cycle led to *irreversible* loss of the original worm morphology for the eight worm dispersions denoted by the filled red squares within the phase diagram shown in Figure 2. To assess the change in storage (G') and loss (G'') moduli with temperature, oscillatory rheology experiments were conducted on three of these [x PEG_{45} + z PEG_{113}] - $PHPMA_{200}$ worm dispersions, where x =

0.00, 0.20 and 0.40 (Figure 3). Viscous liquids (rather than true gels) were observed at 25 °C for x = 0.00 and 0.20, since G'' exceeds G' at this temperature. Cooling to 14 °C resulted in higher viscosities and maximum G' values of 21 Pa (x = 0.00) and 34 Pa (x = 0.20) respectively, which is consistent with the rheological behavior of similar PEG_{113}-$PHPMA_{200}$ worms.[46]

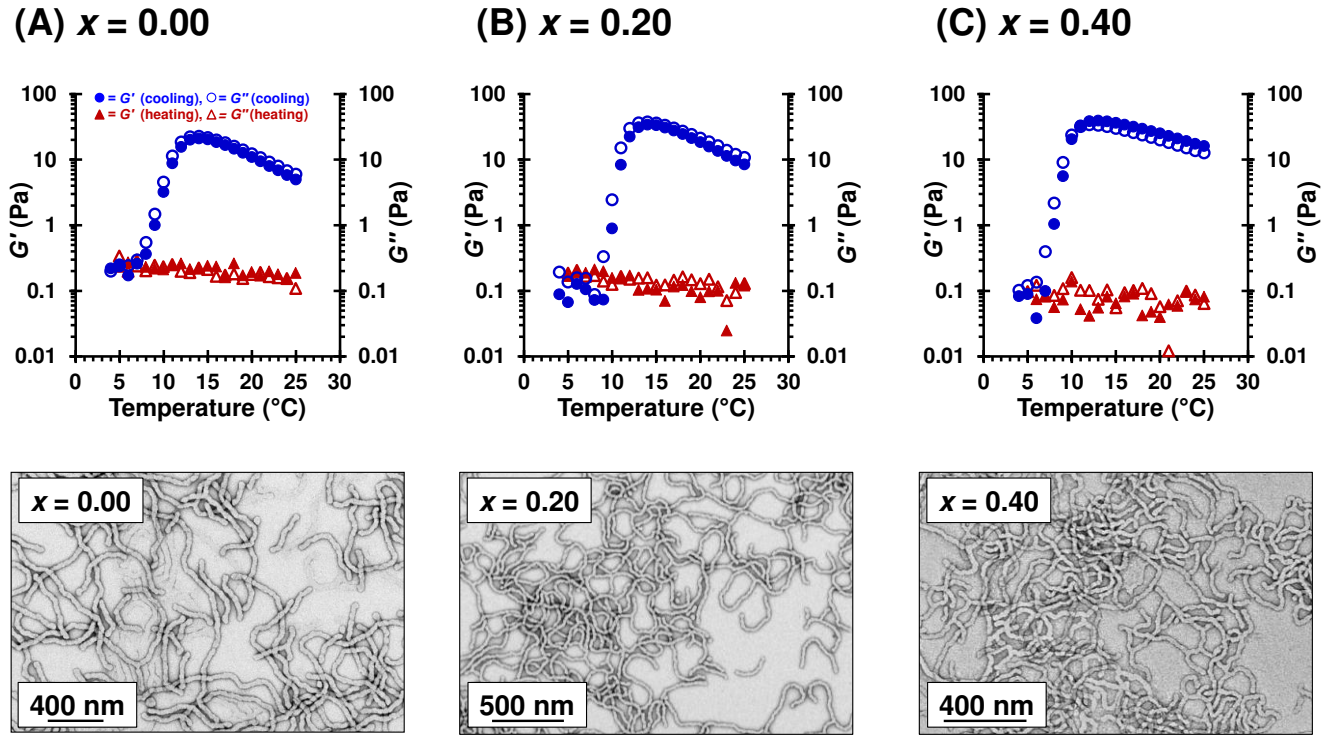

Figure 3. Variation in G' (filled symbols) and G'' (open symbols) with temperature for 10% w/w aqueous dispersions of [x PEG_{45} + z PEG_{113}] – $PHPMA_{200}$ worms where (A) x = 0.00, (B) x = 0.20 and (C) x = 0.40. The blue circles represent data acquired during cooling from 25 °C to 4 °C and the red triangles where obtained on heating from 4 °C to 25 °C. Measurements were conducted at an angular frequency of 1.0 rad s^{-1} at an applied strain of 1.0%. An equilibration time of 10 min was allowed before acquiring each data point. Representative TEM images of the as-synthesized worms that were present prior to this thermal cycle are shown below the corresponding rheology data set.

Further cooling to 4 °C resulted in a dramatic reduction in G' and G'' by approximately two orders of magnitude owing to a worm-to-sphere transition.[46] On increasing x to 0.40, the initial G' value exceeded that of G''; the resulting weak gel had a storage modulus of 16 Pa at 25 °C. Therefore, increasing the proportion of PEG_{45} in the diblock composition for a fixed core DP resulted in an increase in G'. Previous work on PGMA-PHPMA worm gels[67] indicated that G' increases on approaching the worm/vesicle phase boundary, which is consistent with the rheological data observed here. Like the other two worm dispersions shown in Figure 3, initial cooling to 14 °C resulted in an increase in G' to 39 Pa. Further cooling to 4 °C resulted in a comparable dramatic reduction in both G' and G''. The [0.40 PEG_{45} + 0.60 PEG_{113}] – $PHPMA_{200}$ worms exhibited a critical gelation temperature (CGT) of 10 °C, which corresponds to the temperature at which G'' exceeds G'. All three worm dispersions displayed no significant change in G' and G'' on returning from 4 °C to 25 °C (Figure 3; see red triangles data sets).

Visual inspection (tube inversion test) confirmed that only a single worm dispersion exhibited regelation after being subjected a 25 °C – °4 C – 25 °C thermal cycle; this [0.70 PEG_{45} + 0.30 PEG_{113}] - $PHPMA_{115}$ diblock composition is denoted by the open red square data point shown in Figure 2. THF GPC analysis indicated an M_n of 21.9 kg mol^{-1} and a M_w/M_n of 1.13 (these data are expressed relative to PMMA calibration standards; see Figure 4A). TEM studies revealed a pure worm phase at 25 °C (Figure 5). The thermoresponsive behavior of this worm gel was also assessed by oscillatory rheology (Figure 4B). An initial G' of 70 Pa was observed at 25 °C.

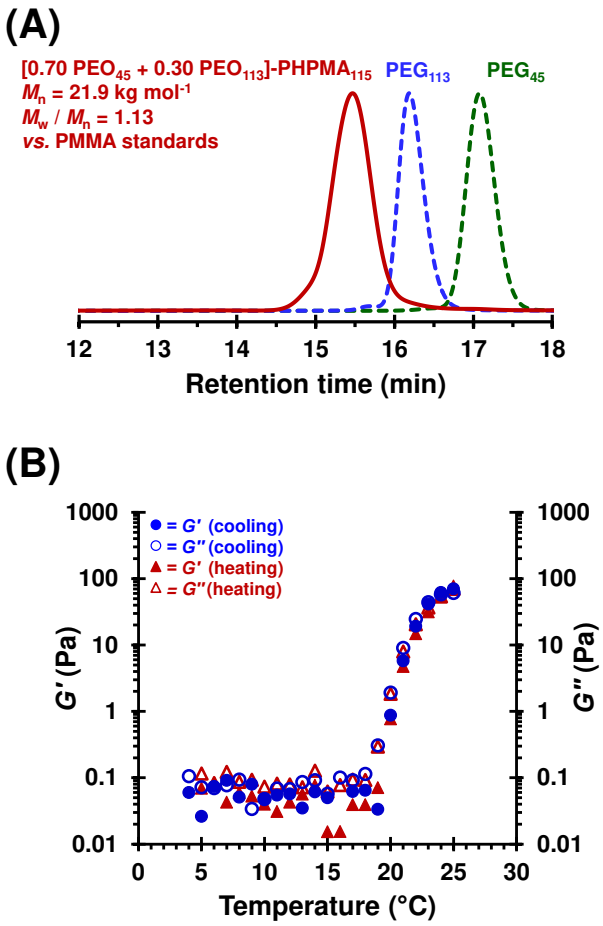

Figure 4. (A) THF GPC chromatogram recorded for a [0.70 PEG_{45} + 0.30 PEG_{113}] - $PHPMA_{115}$ diblock copolymer, and its corresponding PEG_{45} and PEG_{113} macro-CTAs (molecular weight data are expressed relative to PMMA calibration standards). The copolymer molecular weight distribution is both narrow and monomodal and a high blocking efficiency is obtained. (B) Oscillatory rheology data showing the variation in storage (*G′*, filled symbols) and loss (*G″*, open symbols) moduli with temperature as recorded for a 10% w/w aqueous dispersion of [0.70 PEG_{45} + 0.30 PEG_{113}] - $PHPMA_{115}$ worms. Blue circles represent cooling from 25 °C to 4 °C, while red triangles represent heating from 4 °C to 25 °C. Measurements were conducted at an angular frequency of 1.0 rad s^{-1} at an applied strain of 1.0%. An equilibration time of 10 min was allowed before acquiring each data point.

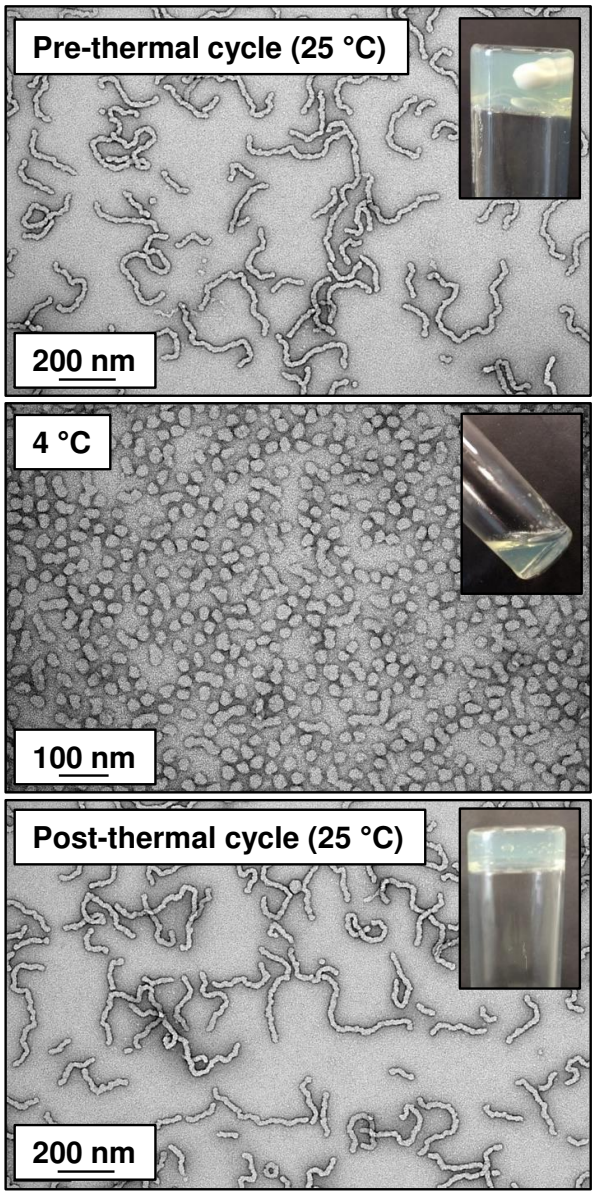

Figure 5. (A) Representative TEM images recorded for dried 0.1% w/w aqueous copolymer dispersions and digital photographs (see insets) obtained for [0.70 PEG_{45} + 0.30 PEG_{113}] - $PHPMA_{115}$: (a) original worms synthesized at 25 °C, (b) spheres formed at 4 °C and (c) reconstituted worms after returning to 25 °C.

Unlike the three worm dispersions described earlier, cooling this worm gel did *not* result in an initial increase in G'. Instead, cooling to 18 °C resulted in a rapid reduction in both G' and G'', with a CGT of 23 °C being observed. Further cooling to 4 °C led to no significant further change

in either G' or G''. TEM studies confirmed the anticipated morphological transition from pure worms at 25 °C to mainly spherical nanoparticles (plus minor populations dimers and trimers)[39] at 4 °C (Figure 5). Dynamic light scattering data obtained at 4 °C revealed an intensity-average particle diameter of 36 nm with a polydispersity index of 0.08, which is consistent with the TEM image in Figure 5b. This substantial reduction in particle anisotropy explains why degelation occurs: the percolation threshold concentration for sphere-sphere contact is much higher than that for worm-worm contact (and the former concentration is higher than the 10% w/w concentration at which these copolymer nanoparticles were synthesized).[38] Warming from 4 °C to 25 °C resulted in minimal hysteresis, and a comparable final G' value of 77 Pa at 25 °C was obtained, thus essentially the same worm gel is reconstituted. TEM analysis performed after this thermal cycle revealed that the original worm morphology was regained. Thus, using a judicious binary mixture of 0.70 PEG_{45} and 0.30 PEG_{113} macro-CTAs for the RAFT aqueous dispersion polymerization of HPMA provides convenient access to a diblock copolymer worm gel that undergoes *thermoreversible (de)gelation* (Scheme 2).

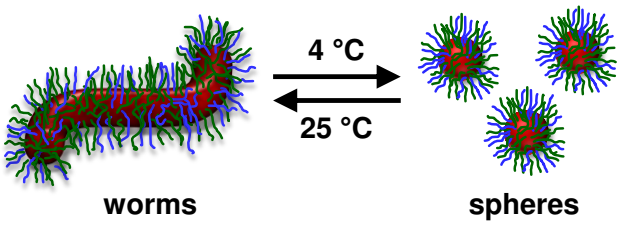

Scheme 2. Schematic cartoon for the *thermoreversible* worm-to-sphere transition observed for a 10% w/w aqueous dispersion of [0.70 PEG_{45} + 0.30 PEG_{113}] – $PHPMA_{115}$ worms. This results in degelation at 4 °C and regelation at 25 °C.

More specifically, such thermoreversible behavior only occurs for a PEG_{45}-rich diblock composition. This is understandable, because this shorter macro-CTA confers weaker steric stabilization, which in turn enables the 1D fusion of multiple spheres to occur much more readily within a relatively short experimental time scale. On the other hand, 30 mol % PEG_{113} macro-CTA is required to prevent the macroscopic precipitation that occurs if the PEG_{45} macro-CTA is used as the sole stabilizer block. Unfortunately, heating a 10% w/w aqueous dispersion of [0.70 PEG_{45} + 0.30 PEG_{113}] - $PHPMA_{115}$ worms from 25 °C to 37 °C resulted in a G' of ≈ 1200 Pa, which is most likely too high to induce stem cell stasis (Figure S4). Moreover, visual inspection indicated significant precipitation at 37 °C. This problem was addressed by lowering the target DP for the PHPMA block in order to reduce its weakly hydrophobic character[68] and hence raise its CGT.[67] Thus, a [0.70 PEG_{45} + 0.30 PEG_{113}] - $PHPMA_{75}$ diblock copolymer was prepared at 10% w/w in deionized water. ^{1}H NMR spectroscopy studies confirmed more than 99% HPMA conversion and THF GPC analysis indicated a unimodal molecular weight distribution, with an M_n = 15.1 kg mol^{-1} and M_w/M_n of 1.12 relative to PMMA calibration standards (Figure 6A). Rheological studies indicated that this diblock composition afforded *thermoreversible* (de)gelation with a CGT of approximately 33 °C and a bulk modulus of 70 Pa at physiological temperature (see Figure S5).

So far, the rheological properties of these block copolymer nanoparticles have been assessed for aqueous dispersions prepared using deionized water. However, for the planned stem cell experiments it is essential to study their rheological behavior when dispersed in a commercial cell culture medium (*Nutristem*).

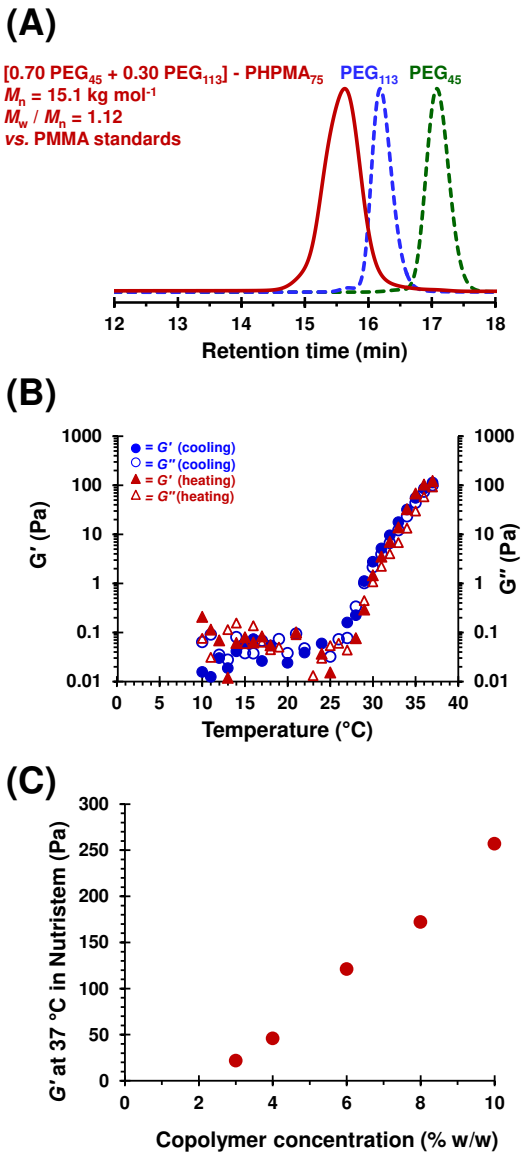

Figure 6. (A) THF GPC chromatogram recorded for a [0.70 PEG_{45} + 0.30 PEG_{113}] - $PHPMA_{75}$ diblock copolymer and its corresponding PEG_{45} and PEG_{113} macro-CTAs (molecular weight data are expressed relative to PMMA calibration standards). The copolymer molecular weight distribution is both narrow and monomodal and a high blocking efficiency is obtained. (B) Oscillatory rheology data showing the variation in storage (*G'*, filled symbols) and loss (*G''*, open symbols) moduli with temperature as recorded for a 6 % w/w aqueous dispersion of [0.70 PEG_{45} + 0.30 PEG_{113}] - $PHPMA_{75}$ worms dispersed in *Nutristem*. Red triangles represent heating from

10 °C to 37 °C and blue circles represent cooling from 37 °C to 10 °C. Measurements were conducted at an angular frequency of 1.0 rad s^{-1} at an applied strain of 1.0%. An equilibration time of 2 min was allowed before acquiring each data point and the first data point was recorded at 10 °C using a pre-chilled rheometer. (C) Variation of *G′* recorded at 37 °C *vs.* copolymer concentration for the same [0.70 PEG_{45} + 0.30 PEG_{113}] - $PHPMA_{75}$ dispersed in *Nutristem*. This linear relationship allows convenient tuning of the gel strength.

Hence the protocol reported by Kocik *et al.*[69] was implemented to transfer the [0.70 PEG_{45} + 0.30 PEG_{113}] – $PHPMA_{75}$ worms from an aqueous dispersion into *Nutristem*. Firstly, the original 10% w/w aqueous dispersion was freeze-dried to yield a pale yellow powder, which was then redispersed with the aid of magnetic stirring at copolymer concentrations ranging between 3% and 10% w/w in *Nutristem* at 4 °C for 3 h. The resulting free-flowing fluids were then allowed to warm up to room temperature.The rheological behavior for a 6% w/w [0.70 PEG_{45} + 0.30 PEG_{113}] - $PHPMA_{75}$ dispersion in *Nutristem* is displayed in Figure 6B. It is perhaps worth noting that the 10 °C to 37 °C heating cycle was performed *before* the 37 °C to 10 °C cooling cycle in order to mimic the temperature profile to which this block copolymer would be exposed during stem cell experiments. Initially, a free-flowing liquid was obtained at 10 °C with a very low *G′* of 0.05 - 0.1 Pa, which remained approximately constant on heating up to 28 °C. Further heating led to a significant increase in gel strength, with a *G′* of 120 Pa being obtained at 37 °C. This temperature-dependent behavior is highly reversible, with little or no hysteresis being observed on cooling to 10 °C. Furthermore, the bulk modulus at 37 °C can be conveniently tuned from 20 Pa to 260 Pa simply by varying the copolymer concentration from 3% w/w to 10% w/w (see Figure 6C). In principle, this binary PEG formulation can be simplified by using a *single* PEG macro-CTA with an appropriate DP. The effective PEG molecular weight of the binary [0.70

PEG_{45} + 0.30 PEG_{113}] stabilizer block is estimated to be 3200 g mol^{-1}, which corresponds to a single PEG block with a mean DP of 65. Therefore, it is hypothesized that a PEG_{65}-$PHPMA_n$ diblock copolymer should also exhibit the desired thermoreversible (de)gelation behavior in *Nutristem*. We intend to examine this hypothesis in the near future.

CONCLUSIONS

Two PEG macro-CTAs with mean DPs of 45 and 113 were synthesized *via* Steglich esterification. This pair of macro-CTAs was employed in varying proportions for the synthesis of diblock copolymer nanoparticles *via* RAFT aqueous dispersion polymerization of HPMA at 50 °C. Such PISA syntheses afforded well-defined [*x* PEG_{45} + *z* PEG_{113}] - $PHPMA_n$ spheres, worms or vesicles, and a phase diagram was constructed to elucidate the relationship between diblock copolymer composition and copolymer morphology. In particular, diblock copolymer worms were targeted that would exhibit appropriate thermoresponsive behavior in aqueous solution. More specifically, when cooled to 4 °C these worms should undergo a thermoreversible morphology transition to form spheres owing to surface plasticization of the PHPMA cores. Unfortunately, this morphological transition proved to be *irreversible* for the majority of the diblock copolymer worms that were synthesized. However, the phase diagram facilitated identification of a *single* diblock copolymer composition that exhibited the desired thermoreversible behavior. Both TEM and rheology studies indicated that essentially the same worms (and gels) were reconstituted after a 25 °C - 4 °C - 25 °C thermal cycle. Moreover, further optimization of the diblock copolymer composition enabled thermoreversible gelation to be achieved in the presence of a commercial stem cell culture medium. Thus [0.70 PEG_{45} + 0.30 PEG_{113}] - $PHPMA_{75}$ diblock copolymer worms formed soft free-standing gels at 37 °C on

redispersing the freeze-dried copolymer powder in *Nutristem*. Furthermore, simply adjusting the copolymer concentration enabled the gel strength to be conveniently tuned at 37 °C. In future work, this new PEG-based PISA formulation should enable the question of the importance of hydroxyl functionality in the induction of stem cell stasis to be addressed.

ASSOCIATED CONTENT

Supporting Information.

The Supporting Information is available free of charge at http://pubs.acs.org/. Full experimental and analytical details, supplementary schematics and figures.

AUTHOR INFORMATION

Corresponding Author

*E-mail: s.p.armes@sheffield.ac.uk (SPA), n.penfold@sheffield.ac.uk (NJWP)

Author Contributions

The manuscript was written through contributions of NJWP and SPA authors. NJWP and SPA designed the experiments. NJWP and JW performed the experiments. All authors have given approval to the final version of the manuscript.

Notes

The authors declare no competing financial interest

ACKNOWLEDGMENTS

SPA acknowledges an ERC *Advanced Investigator* grant (PISA 320372) and the EPSRC for an *Established Career* Particle Technology Fellowship (EP/R003009). These grants were used to provide post-doctoral support for NJWP.

REFERENCES

(1) Wang, X.; An, Z. New Insights into RAFT Dispersion Polymerization-Induced Self-Assembly: From Monomer Library, Morphological Control, and Stability to Driving Forces. *Macromol. Rapid Commun.* **2018**, e1800325.
(2) Yeow, J.; Boyer, C. Photoinitiated Polymerization-Induced Self-Assembly (Photo-PISA): New Insights and Opportunities. *Advanced Science* **2017**, *4*, e1700137
(3) Derry, M. J.; Fielding, L. A.; Armes, S. P. Polymerization-induced self-assembly of block copolymer nanoparticles via RAFT non-aqueous dispersion polymerization. *Prog. Polym. Sci.* **2016**, *52*, 1-18.
(4) Warren, N. J.; Armes, S. P. Polymerization-induced self-assembly of block copolymer nano-objects via RAFT aqueous dispersion polymerization. *J. Am. Chem. Soc* **2014**, *136*, 10174-10185.
(5) Canning, S. L.; Smith, G. N.; Armes, S. P. A Critical Appraisal of RAFT-Mediated Polymerization-Induced Self-Assembly. *Macromolecules* **2016**, *49*, 1985-2001.
(6) Rieger, J. Guidelines for the Synthesis of Block Copolymer Particles of Various Morphologies by RAFT Dispersion Polymerization. *Macromol. Rapid Commun.* **2015**, *36*, 1458-1471.
(7) Charleux, B.; Delaittre, G.; Rieger, J.; D'Agosto, F. Polymerization-Induced Self-Assembly: From Soluble Macromolecules to Block Copolymer Nano-Objects in One Step. *Macromolecules* **2012**, *45*, 6753-6765.
(8) Khor, S. Y.; Quinn, J. F.; Whittaker, M. R.; Truong, N. P.; Davis, T. P. Controlling Nanomaterial Size and Shape for Biomedical Applications via Polymerization-Induced Self-Assembly. *Macromol. Rapid Commun.* **2018**, e1800438.
(9) Zhao, W.; Gody, G.; Dong, S.; Zetterlund, P. B.; Perrier, S. Optimization of the RAFT polymerization conditions for the in situ formation of nano-objects via dispersion polymerization in alcoholic medium. *Polym. Chem.* **2014**, *5*, 6990-7003.
(10) Zetterlund, P. B.; Thickett, S. C.; Perrier, S.; Bourgeat-Lami, E.; Lansalot, M. Controlled/Living Radical Polymerization in Dispersed Systems: An Update. *Chem. Rev.* **2015**, *115*, 9745-9800.
(11) Pei, Y.; Lowe, A. B.; Roth, P. J. Stimulus-Responsive Nanoparticles and Associated (Reversible) Polymorphism via Polymerization Induced Self-assembly (PISA). *Macromol. Rapid Commun.* **2017**, *38*, 1600528.
(12) Wang, X.; Shen, L.; An, Z. Dispersion polymerization in environmentally benign solvents via reversible deactivation radical polymerization. *Prog. Polym. Sci.* **2018**, *83*, 1-27.
(13) Chiefari, J.; Chong, Y. K.; Ercole, F.; Krstina, J.; Jeffery, J.; Le, T. P. T.; Mayadunne, R. T. A.; Meijs, G. F.; Moad, C. L.; Moad, G.; Rizzardo, E.; Thang, S. H. Living Free-Radical Polymerization by Reversible Addition−Fragmentation Chain Transfer: The RAFT Process. *Macromolecules* **1998**, *31*, 5559-5562.

(14) Moad, G.; Rizzardo, E.; Thang, S. H. Living Radical Polymerization by the RAFT Process - A Third Update. *Aust. J. Chem.* **2012**, *65*, 985-1076.
(15) Moad, G. RAFT polymerization to form stimuli-responsive polymers. *Polym. Chem.* **2017**, *8*, 177-219.
(16) Perrier, S. 50th Anniversary Perspective: RAFT Polymerization—A User Guide. *Macromolecules* **2017**, *50*, 7433-7447.
(17) Hill, M. R.; Carmean, R. N.; Sumerlin, B. S. Expanding the Scope of RAFT Polymerization: Recent Advances and New Horizons. *Macromolecules* **2015**, *48*, 5459-5469.
(18) Boyer, C.; Stenzel, M. H.; Davis, T. P. Building nanostructures using RAFT polymerization. *J. Polym. Sci. A Polym. Chem.* **2011**, *49*, 551-595.
(19) Wang, K.; Wang, Y.; Zhang, W. Synthesis of diblock copolymer nano-assemblies by PISA under dispersion polymerization: comparison between ATRP and RAFT. *Polym. Chem.* **2017**, *8*, 6407-6415.
(20) Wang, G.; Wang, Z.; Lee, B.; Yuan, R.; Lu, Z.; Yan, J.; Pan, X.; Song, Y.; Bockstaller, M. R.; Matyjaszewski, K. Polymerization-induced self-assembly of acrylonitrile via ICAR ATRP. *Polymer* **2017**, *129*, 57-67.
(21) Wang, J.; Wang, G.; Wang, J.; Wu, Z.; Matyjaszewski, K. In Situ Crosslinking of Nanoparticles in Polymerization-Induced Self-Assembly via ARGET ATRP of Glycidyl Methacrylate. *Macromol. Rapid Commun.* **2018**, e1800332.
(22) Wang, G.; Schmitt, M.; Wang, Z.; Lee, B.; Pan, X.; Fu, L.; Yan, J.; Li, S.; Xie, G.; Bockstaller, M. R.; Matyjaszewski, K. Polymerization-Induced Self-Assembly (PISA) Using ICAR ATRP at Low Catalyst Concentration. *Macromolecules* **2016**, *49*, 8605-8615.
(23) Wright, D. B.; Touve, M. A.; Adamiak, L.; Gianneschi, N. C. ROMPISA: Ring-Opening Metathesis Polymerization-Induced Self-Assembly. *ACS Macro Lett.* **2017**, *6*, 925-929.
(24) Torres-Rocha, O. L.; Wu, X.; Zhu, C.; Crudden, C. M.; Cunningham, M. F. Polymerization-Induced Self-Assembly (PISA) of 1,5-Cyclooctadiene Using Ring Opening Metathesis Polymerization. *Macromol. Rapid Commun.* **2018**, e1800326.
(25) Torres-Rocha, O. L.; Zhu, C.; Cunningham, M. F.; Wu, X.; Crudden, C. M. Polymerization-Induced Self-Assembly (PISA) of 1,5-Cyclooctadiene Using Ring Opening Metathesis Polymerization. *Macromol. Rapid Commun.* **2018**, e1800326.
(26) Delaittre, G.; Save, M.; Gaborieau, M.; Castignolles, P.; Rieger, J.; Charleux, B. Synthesis by nitroxide-mediated aqueous dispersion polymerization, characterization, and physical core-crosslinking of pH- and thermoresponsive dynamic diblock copolymer micelles. *Polym. Chem.* **2012**, *3*, 1526-1538.
(27) Qiao, X. G.; Dugas, P. Y.; Charleux, B.; Lansalot, M.; Bourgeat-Lami, E. Nitroxide-mediated polymerization-induced self-assembly of amphiphilic block copolymers with a pH/temperature dual sensitive stabilizer block. *Polym. Chem.* **2017**, *8*, 4014-4029.
(28) Darabi, A.; Jessop, P. G.; Cunningham, M. F. One-Pot Synthesis of Poly((diethylamino)ethyl methacrylate-co-styrene)-b-poly(methyl methacrylate-co-styrene) Nanoparticles via Nitroxide-Mediated Polymerization. *Macromolecules* **2015**, *48*, 1952-1958.
(29) Qiao, X. G.; Lansalot, M.; Bourgeat-Lami, E.; Charleux, B. Nitroxide-Mediated Polymerization-Induced Self-Assembly of Poly(poly(ethylene oxide) methyl ether methacrylate-co-styrene)-b-poly(n-butyl methacrylate-co-styrene) Amphiphilic Block Copolymers. *Macromolecules* **2013**, *46*, 4285-4295.

(30) Groison, E.; Brusseau, S.; D'Agosto, F.; Magnet, S.; Inoubli, R.; Couvreur, L.; Charleux, B. Well-Defined Amphiphilic Block Copolymer Nanoobjects via Nitroxide-Mediated Emulsion Polymerization. *ACS Macro Lett.* **2012**, *1*, 47-51.
(31) Cunningham, V. J.; Alswieleh, A. M.; Thompson, K. L.; Williams, M.; Leggett, G. J.; Armes, S. P.; Musa, O. M. Poly(glycerol monomethacrylate)-poly(benzyl methacrylate) diblock copolymer nanoparticles via RAFT emulsion polymerization: Synthesis, characterization, and interfacial activity. *Macromolecules* **2014**, *47*, 5613-5623.
(32) Blanazs, A.; Madsen, J.; Battaglia, G.; Ryan, A. J.; Armes, S. P. Mechanistic insights for block copolymer morphologies: how do worms form vesicles? *J. Am. Chem. Soc* **2011**, *133*, 16581-16587.
(33) Gyorgy, C.; Lovett, J. R.; Penfold, N. J. W.; Armes, S. P. Epoxy-Functional Sterically Stabilized Diblock Copolymer Nanoparticles via RAFT Aqueous Emulsion Polymerization: Comparison of Two Synthetic Strategies. *Macromol. Rapid Commun.* **2018**, e1800289.
(34) Hatton, F. L.; Lovett, J. R.; Armes, S. P. Synthesis of well-defined epoxy-functional spherical nanoparticles by RAFT aqueous emulsion polymerization. *Polym. Chem.* **2017**, *8*, 4856-4868.
(35) Khor, S. Y.; Truong, N. P.; Quinn, J. F.; Whittaker, M. R.; Davis, T. P. Polymerization-Induced Self-Assembly: The Effect of End Group and Initiator Concentration on Morphology of Nanoparticles Prepared via RAFT Aqueous Emulsion Polymerization. *ACS Macro Lett.* **2017**, *6*, 1013-1019.
(36) Cockram, A. A.; Neal, T. J.; Derry, M. J.; Mykhaylyk, O. O.; Williams, N. S. J.; Murray, M. W.; Emmett, S. N.; Armes, S. P. Effect of Monomer Solubility on the Evolution of Copolymer Morphology during Polymerization-Induced Self-Assembly in Aqueous Solution. *Macromolecules* **2017**, *50*, 796-802.
(37) Blanazs, A.; Ryan, A. J.; Armes, S. P. Predictive Phase Diagrams for RAFT Aqueous Dispersion Polymerization: Effect of Block Copolymer Composition, Molecular Weight, and Copolymer Concentration. *Macromolecules* **2012**, *45*, 5099-5107.
(38) Lovett, J. R.; Derry, M. J.; Yang, P.; Hatton, F. L.; Warren, N. J.; Fowler, P. W.; Armes, S. P. Can percolation theory explain the gelation behavior of diblock copolymer worms? *Chem. Sci.* **2018**, *9*, 7138-7144.
(39) Blanazs, A.; Verber, R.; Mykhaylyk, O. O.; Ryan, A. J.; Heath, J. Z.; Douglas, C. W.; Armes, S. P. Sterilizable gels from thermoresponsive block copolymer worms. *J. Am. Chem. Soc* **2012**, *134*, 9741-9748.
(40) Simon, K. A.; Warren, N. J.; Mosadegh, B.; Mohammady, M. R.; Whitesides, G. M.; Armes, S. P. Disulfide-based diblock copolymer worm gels: A wholly-synthetic thermoreversible 3D matrix for sheet-based cultures. *Biomacromolecules* **2015**, *16*, 3952-3958.
(41) Canton, I.; Warren, N. J.; Chahal, A.; Amps, K.; Wood, A.; Weightman, R.; Wang, E.; Moore, H.; Armes, S. P. Mucin-Inspired Thermoresponsive Synthetic Hydrogels Induce Stasis in Human Pluripotent Stem Cells and Human Embryos. *ACS Cent. Sci.* **2016**, *2*, 65-74.
(42) Tan, J.; Liu, D.; Bai, Y.; Huang, C.; Li, X.; He, J.; Xu, Q.; Zhang, X.; Zhang, L. An insight into aqueous photoinitiated polymerization-induced self-assembly (photo-PISA) for the preparation of diblock copolymer nano-objects. *Polym. Chem.* **2017**, *8*, 1315-1327.
(43) Tan, J.; Liu, D.; Zhang, X.; Huang, C.; He, J.; Xu, Q.; Li, X.; Zhang, L. Facile preparation of hybrid vesicles loaded with silica nanoparticles via aqueous photoinitiated polymerization-induced self-assembly. *RSC Adv.* **2017**, *7*, 23114-23121.

(44) Ren, K.; Perez-Mercader, J. Thermoresponsive gels directly obtained via visible light-mediated polymerization-induced self-assembly with oxygen tolerance. *Polym. Chem.* **2017**, *8*, 3548-3552.
(45) Touve, M. A.; Figg, C. A.; Wright, D. B.; Park, C.; Cantlon, J.; Sumerlin, B. S.; Gianneschi, N. C. Polymerization-Induced Self-Assembly of Micelles Observed by Liquid Cell Transmission Electron Microscopy. *ACS Cent. Sci.* **2018**, *4*, 543-547.
(46) Warren, N. J.; Mykhaylyk, O. O.; Mahmood, D.; Ryan, A. J.; Armes, S. P. RAFT aqueous dispersion polymerization yields poly(ethylene glycol)-based diblock copolymer nano-objects with predictable single phase morphologies. *J. Am. Chem. Soc* **2014**, *136*, 1023-1033.
(47) Blackman, L. D.; Doncom, K. E. B.; Gibson, M. I.; O'Reilly, R. K. Comparison of photo- and thermally initiated polymerization-induced self-assembly: a lack of end group fidelity drives the formation of higher order morphologies. *Polym. Chem.* **2017**, *8*, 2860-2871.
(48) Blackman, L. D.; Varlas, S.; Arno, M. C.; Fayter, A.; Gibson, M. I.; Oreilly, R. K. Permeable Protein-Loaded Polymersome Cascade Nanoreactors by Polymerization-Induced Self-Assembly. *ACS Macro Lett.* **2017**, *6*, 1263-1267.
(49) Blackman, L. D.; Varlas, S.; Arno, M. C.; Houston, Z. H.; Fletcher, N. L.; Thurecht, K. J.; Hasan, M.; Gibson, M. I.; O'Reilly, R. K. Confinement of Therapeutic Enzymes in Selectively Permeable Polymer Vesicles by Polymerization-Induced Self-Assembly (PISA) Reduces Antibody Binding and Proteolytic Susceptibility. *ACS Cent. Sci.* **2018**, *4*, 718-723.
(50) Tan, J.; Sun, H.; Yu, M.; Sumerlin, B. S.; Zhang, L. Photo-PISA: Shedding Light on Polymerization-Induced Self-Assembly. *ACS Macro Lett.* **2015**, *4*, 1249-1253.
(51) Zaquen, N.; Yeow, J.; Junkers, T.; Boyer, C.; Zetterlund, P. B. Visible Light-Mediated Polymerization-Induced Self-Assembly Using Continuous Flow Reactors. *Macromolecules* **2018**, *51*, 5165-5172.
(52) Semsarilar, M.; Ladmiral, V.; Blanazs, A.; Armes, S. P. Anionic polyelectrolyte-stabilized nanoparticles via RAFT aqueous dispersion polymerization. *Langmuir* **2012**, *28*, 914-922.
(53) Semsarilar, M.; Ladmiral, V.; Blanazs, A.; Armes, S. P. Cationic polyelectrolyte-stabilized nanoparticles via RAFT aqueous dispersion polymerization. *Langmuir* **2013**, *29*, 7416-7424.
(54) Penfold, N. J. W.; Ning, Y.; Verstraete, P.; Smets, J.; Armes, S. P. Cross-Linked Cationic Diblock Copolymer Worms are Superflocculants for Micrometer-sized Silica Particles. *Chem. Sci.* **2016**, *7*, 6894-6904.
(55) Penfold, N. J. W.; Parnell, A. J.; Molina, M.; Verstraete, P.; Smets, J.; Armes, S. P. Layer-By-Layer Self-Assembly of Polyelectrolytic Block Copolymer Worms on a Planar Substrate. *Langmuir* **2017**, *33*, 14425-14436.
(56) Williams, M.; Penfold, N. J. W.; Armes, S. P. Cationic and reactive primary amine-stabilised nanoparticles via RAFT aqueous dispersion polymerisation. *Polym. Chem.* **2016**, *7*, 384-393.
(57) Williams, M.; Penfold, N. J. W.; Lovett, J. R.; Warren, N. J.; Douglas, C. W. I.; Doroshenko, N.; Verstraete, P.; Smets, J.; Armes, S. P. Bespoke cationic nano-objects via RAFT aqueous dispersion polymerisation. *Polym. Chem.* **2016**, *7*, 3864-3873.
(58) Gonzato, C.; Semsarilar, M.; Jones, E. R.; Li, F.; Krooshof, G. J. P.; Wyman, P.; Mykhaylyk, O. O.; Tuinier, R.; Armes, S. P. Rational Synthesis of Low-Polydispersity Block Copolymer Vesicles in Concentrated Solution via Polymerization-Induced Self-Assembly. *J. Am. Chem. Soc* **2014**, *136*, 11100-11106.

(59) Tan, J.; Li, X.; Zeng, R.; Liu, D.; Xu, Q.; He, J.; Zhang, Y.; Dai, X.; Yu, L.; Zeng, Z.; Zhang, L. Expanding the Scope of Polymerization-Induced Self-Assembly: Z-RAFT-Mediated Photoinitiated Dispersion Polymerization. *ACS Macro Lett.* **2018**, *7*, 255-262.
(60) Sugihara, S.; Ma'Radzi, A. H.; Ida, S.; Irie, S.; Kikukawa, T.; Maeda, Y. In situ nano-objects via RAFT aqueous dispersion polymerization of 2-methoxyethyl acrylate using poly(ethylene oxide) macromolecular chain transfer agent as steric stabilizer. *Polymer* **2015**, *76*, 17-24.
(61) Rieger, J.; Grazon, C.; Charleux, B.; Alaimo, D.; Jerome, C. Pegylated thermally responsive block copolymer micelles and nanogels via in situ RAFT aqueous dispersion polymerization. *J. Polym. Sci. A Polym. Chem.* **2009**, *47*, 2373-2390.
(62) Gao, C.; Zhou, H.; Qu, Y.; Wang, W.; Khan, H.; Zhang, W. In Situ Synthesis of Block Copolymer Nanoassemblies via Polymerization-Induced Self-Assembly in Poly(ethylene glycol). *Macromolecules* **2016**, *49*, 3789-3798.
(63) Tan, J.; Xu, Q.; Zhang, Y.; Huang, C.; Li, X.; He, J.; Zhang, L. Room Temperature Synthesis of Self-Assembled AB/B and ABC/BC Blends by Photoinitiated Polymerization-Induced Self-Assembly (Photo-PISA) in Water. *Macromolecules* **2018**, *51*, 7396-7406.
(64) Wang, X.; Figg, C. A.; Lv, X.; Yang, Y.; Sumerlin, B. S.; An, Z. Star Architecture Promoting Morphological Transitions during Polymerization-Induced Self-Assembly. *ACS Macro Lett.* **2017**, *6*, 337-342.
(65) Bailey, F. E., Jr.; Callard, R. W. Properties of poly(ethylene oxide) in aqueous solution. *J. Appl. Polym. Sci.* **1959**, *1*, 56-62.
(66) Israelachvili, J. N.; Mitchell, D. J.; Ninham, B. W. Theory of self-assembly of hydrocarbon amphiphiles into micelles and bilayers. *J. Chem. Soc., Faraday Trans. 2* **1976**, *72*, 1525-1568.
(67) Verber, R.; Blanazs, A.; Armes, S. P. Rheological studies of thermo-responsive diblock copolymer worm gels. *Soft Matter* **2012**, *8*, 9915-9922.
(68) Warren, N. J.; Derry, M. J.; Mykhaylyk, O. O.; Lovett, J. R.; Ratcliffe, L. P. D.; Ladmiral, V.; Blanazs, A.; Fielding, L. A.; Armes, S. P. Critical Dependence of Molecular Weight on Thermoresponsive Behavior of Diblock Copolymer Worm Gels in Aqueous Solution. *Macromolecules* **2018**, *51*, 8357-8371.
(69) Kocik, M. K.; Mykhaylyk, O. O.; Armes, S. P. Aqueous worm gels can be reconstituted from freeze-dried diblock copolymer powder. *Soft Matter* **2014**, *10*, 3984-3992.